The Toggle Switch Model for Gene Expression Change during the Prenatal-to-Postnatal Transition in Mammals

Junjun Hao,[1] Wuling Hao,[2] Zhen Liu,*[,1] and Peng Shi*[,1,3,4]

[1]State Key Laboratory of Genetic Resources and Evolution, Kunming Institute of Zoology, Chinese Academy of Sciences, Kunming, China

[2]College of Mathematics, Yunnan Normal University, Kunming, China

[3]School of Future Technology, University of Chinese Academy of Sciences, Beijing, China

[4]Center for Excellence in Animal Evolution and Genetics, Chinese Academy of Sciences, Kunming, China

***Corresponding authors:** E-mails: zhenliu@mail.kiz.ac.cn; ship@mail.kiz.ac.cn.

Associate editor: Naruya Saitou

Abstract

The prenatal-to-postnatal transition is a pivotal process in the life cycle whereby an organism shifts from responding to intrauterine cues to undergoing extrauterine stresses with many physiological adaptations. However, the molecular basis underlying the evolutionarily conserved physiological adaptations remains elusive. Here, we analyze the transcriptomes of seven organs across developmental time points from five mammalian species by constructing computational coexpression networks and report a developmental shift of gene expression at the perinatal stage. The low-to-high and high-to-low expressed genes tightly coalesce in the functional categories and gene regulatory pathways that implicate the physiological adaptions during the prenatal-to-postnatal transition, including lipid metabolism, circadian rhythm, immune response, cell cycle, and cell division. The low-to-high and high-to-low expressed genes around the perinatal stage tend to form the mutually inhibitory toggle switch gene pairs linking the gene regulatory networks in response to the environmental changes. We thus propose the toggle switch model for the developmental shift of gene expression as a mechanic framework to investigate how the physiological adaptations occur during the prenatal-to-postnatal transition.

Key words: **mammal, coexpression network, WGCNA, transcriptome.**

Introduction

The transition from prenatal stages to postnatal stages represents one of the critical events during an organism's development, in which an organism shifts from completely depending on another for life-sustaining oxygen and nutrients to independently facing extrauterine stresses, such as atmospheric oxygen, fatty acids-rich nutrient, light–dark cycle, and foreign microbes (fig. 1*A*). This radical switching requires wide and intense physiological adaptations for the organism, such as cardiovascular adaptation, pulmonary adaptation, and thermal adaptation (Askin 2002).

Of the extrauterine stresses, the change of oxygen concentration is the first challenge that an individual has to experience after birth. For example, mammalian fetuses often develop in hypoxic environments. The arterial and venous oxygen partial pressure (pO_2) of the fetus rarely exceed 30 mmHg, whereas the maternal arterial and venous pO_2 are approximately 90 and 70 mmHg, respectively (Emmanouilides et al. 1995). Exposure of mammalian embryos to atmospheric oxygen (21%) consistently impairs embryonic development (Pabon et al. 1989; Eppig and Wigglesworth 1995; Catt and Henman 2000). Notably, the arterial oxygen saturation rapidly increases from approximately 60% of the fetuses to >90% of the newborns with the normal postnatal transition (Oski and Delivoria-Papadopoulos 1971; Harris et al. 1986; Porter 1987; Dimich et al. 1991; Carrasco et al. 1997). The consequence of such a sudden rise in oxygen concentration during the fetal-to-neonatal transition causes a remarkable increase of reactive oxygen species (ROS) and oxidative DNA damage, leading to a permanent cell-cycle arrest and impairing cell division (Puente et al. 2014; Torres-Cuevas et al. 2017; Villamor et al. 2019).

The prenatal-to-postnatal transition is also characterized by nutritional changes. During pregnancy, the mammalian fetuses are supplied through the placental with a diet rich in carbohydrates and amino acids, and glucose is used as a major energy source (Battaglia and Meschia 1978; Platt and Deshpande 2005). Immediately after birth, the maternal supply of glucose ceases abruptly and newborns have to withstand a brief period of starvation before being fed with milk that is a diet high in fat and low in carbohydrates (Girard et al. 1992). The lipid content of milk, as a major energy source of infants, represents approximately 60% of the total calories, whereas the carbohydrate content represents <10% (Girard et al. 1977; Henning 1981). Thus newborns must have developed the metabolic pathways for efficient fatty acid oxidation

Article

to maintain the physiological functions for energy resource transition.

Beyond the changes in oxygen tension and nutrient availability, many additional environmental alternations, such as the light–dark cycle (Honma 2020) and exposure to foreign microbes (Yu et al. 2018), have also occurred during the prenatal-to-postnatal transition (fig. 1A). To cope with these environmental changes, the newborns have evolved wide physiological adaptions in cardiovascular system, pulmonary system, energy metabolisms, immune response, and so on (Girard et al. 1992; Askin 2002; Mota-Rojas et al. 2011). Most of what we know about the molecular basis on these postnatal physiological adaptations have often individually focused on the assessment of hormone abundance, enzyme abundance and catalytic activity, mRNA levels of specific metabolic participants, and regulators (Girard et al. 1973; Asikainen et al. 1998; Han et al. 2009; Hurley et al. 2018). Thus, the molecular basis underlying the evolutionarily conserved prenatal-to-postnatal physiological adaptations lacks systematic examination.

In this study, we analyzed the transcriptome data of seven organs of five mammalian species across developmental time points covering fetal, neonatal, postnatal stages, revealing a general transcriptome-wide change of gene expression around the perinatal stage. By constructing the gene coexpression networks along the developmental stages, we identified the modules that are closely associated with the phenotypic shifts during the prenatal-to-postnatal transition. We assessed the shared biological functions and signaling pathways among the genes within the up- and down-regulated modules, showing their significant associations with the physiological adaptations from fetuses to newborns. Notably, the genes in the up-regulated modules tended to form a mutually inhibitory pair with the genes in the down-regulated modules; we thus propose the toggle switch model as a framework for further investigating the molecular basis underlying the physiological adaptations during the prenatal-to-postnatal transition.

Results and Discussion

Transcriptome-Wide Changes around the Perinatal Stage in Mammals

Given various physiological adaptions for the newborns to cope with new extrauterine stressors, we reasoned that transcriptomic data from organs across developmental time points would inform our understanding of the molecular basis on physiological adaptations during the prenatal-to-postnatal transition, as previous studies suggested (Asikainen et al. 1998; Han et al. 2009; Chapple et al. 2013; Hurley et al. 2018). We collected and compiled 1,425 transcriptomic data sets of seven organs (brain, cerebellum, heart, liver, kidney, ovary, and testes) spanning prenatal and postnatal development time points across five placental mammals human, rhesus macaque, mouse, rat, and rabbit (supplementary table S1, Supplementary Material online) (Cardoso-Moreira et al. 2019). Based on developmentally dynamic gene expression at the transcriptome scale, the mouse-matched stage correspondences are established among these species (Cardoso-Moreira et al. 2019). In the stage correspondences, some key developmental events such as birth exhibit heterochrony of temporal gene expression. For example, the gene expression profiling in a newborn mouse (P0) is closest to a human at embryonic period W19. Before investigating the molecular basis on physiological adaptations during the prenatal-to-postnatal transition, we first explored the global relationship of transcriptomic data across different developmental time points for each organ of each species by performing the principal component analysis (PCA). The results showed that the transcriptomic data of seven organs of five mammalian species generally exhibited an evident turning point along with the second principal component (PC2) (fig. 1B). In the PCAs, PC1 separated the samples from prenatal to postnatal stages and explained approximately 39% variance in gene expression; PC2 generally separated the samples by the difference between the perinatal and other developmental stages, explaining approximately 17% variance in gene expression (supplementary table S2, Supplementary Material online). Thus, the PCA results showed a remarkable gene expression difference at the transcriptomic scale between the prenatal and postnatal stages across different organs of different mammals. Notably, the results for some organs such as the brain, heart, and cerebellum of rhesus macaque were inconsistent with our general observation, which may result from a small sample size at the prenatal stages (supplementary table S1, Supplementary Material online). To examine the robustness of these results, we performed the above analysis for the variably expressed genes across different developmental time points (CV$>$1; supplementary table S2, Supplementary Material online). The expression profiles of the variably expressed genes across developmental stages showed more remarkable turning points between the prenatal and postnatal stages than all expressed genes, further supporting these results (supplementary fig. S1, Supplementary Material online).

Gene Expression Switch around the Perinatal Stage Based on Transcriptome-Wide Coexpression Network Analysis

To identify the genes with evolutionarily conserved expression changes between the prenatal and postnatal stages, we first compiled a data set containing a total of 8,238 one-to-one orthologous protein-coding genes from the above transcriptomic data, covering different development time points across five placental mammals human, rhesus macaque, mouse, rat, and rabbit (supplementary table S3, Supplementary Material online). By applying the signed weighted gene coexpression network analysis (WGCNA) (Langfelder and Horvath 2008) for the data set, we identified a total of 23 coexpression modules that were labeled by different colors by setting the soft-thresholding power 18 (fig. 2A and supplementary fig. S2 and table S4, Supplementary Material online). These modules represent the contained genes sharing a highly similar expression pattern during development across different mammals. To assess the

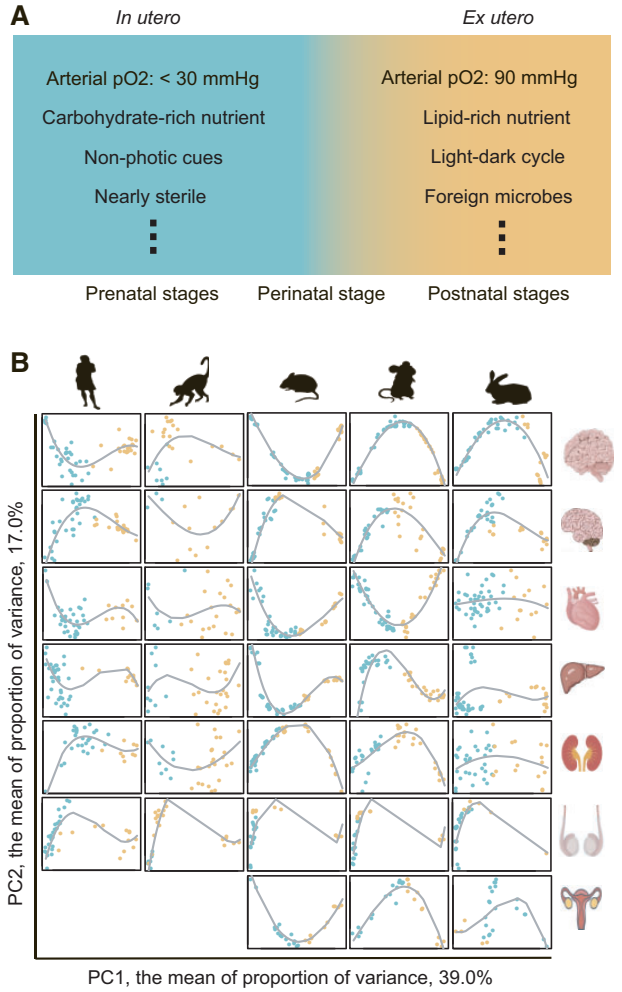

Fig. 1. The switching of environmental factors and gene expression between the prenatal and postnatal stages in mammals. (*A*) Many environmental factors are abruptly changed from *in utero* to *ex utero* in mammals. (*B*) Principal component analysis of transcriptomic data for each of seven organs across five placental mammalian species. The cyan and yellow dots denote the prenatal and postnatal samples, respectively. The lines are from the cubic polynomial fitting.

preservation and reproducibility of the identified 23 modules, we compiled a control data set largely similar to the above data set (supplementary table S5, Supplementary Material online), containing the expression data of the same 8,238 genes from forebrain, heart, liver, and kidney, and spinning mouse E11.5 to 8 weeks (He et al. 2020). Using the modulePreservation function (Langfelder et al. 2011), we found that all 23 modules were significantly preserved ($Z_{summary} > 5$; fig. 2*B*).

Next, we digitized the specificity of each developmental stage (DDS) by respectively assigning "0" and "1" to the developmental stages before and after the stage corresponding to the switch of gene expression. Taking the mouse-matched stage E18.5 as an example, we assigned "0" to the developmental stages before E18.5 (E10.5, E11.5, E12.5, E13.5, E14.5, E15.5, E16.5, and E17.5) and assigned "1" to the developmental stages at and after E18.5 (E18.5, birth, P0, P3, P14, P28, and P63) for representing the specificity of gene expression switching at E18.5 (supplementary table S6, Supplementary Material online). Further, we assessed the correlation between the DDS and the module eigengene (ME) for each module across 14 developmental time points of five placental mammals (fig. 2*C* and supplementary tables S4 and S7, Supplementary Material online). The eigengene, as the first principal component of a module, reflects the general expression pattern of the genes within the module (Langfelder and Horvath 2008). We ranked and numerically labeled the modules according to the values of the Pearson correlation coefficient (*R*) from the most positive correlation module (M1) to the most negative correlation module (M23) at the developmental stage of birth (fig. 2*D*). Of the 14 developmental stages, E18.5, P0, birth, and P3 (i.e., the perinatal stage) exhibited the most significant correlations between the DDS and the ME among 23 coexpression modules compared with other developmental stages (fig. 2*E*). Moreover, the absolute *R* values were generally larger for the perinatal stage than other developmental stages (fig. 2*F*). To test the robustness of the results, we re-examined the relationships between the DDS and ME by estimating the maximal information coefficient (MIC), which is a measure of the strength of the linear or nonlinear association between two variables (Reshef et al. 2011). Similar to the results based on the *R* values, the perinatal stages displayed the most significant correlations between the DDS and the ME among 23 coexpression modules according to the MIC values (supplementary fig. S3, Supplementary Material online).

These results suggest that the switching changes of gene expression at the transcriptomic scale largely occur around the perinatal stage, which may provide insights into understanding the molecular basis of the physiological adaptations during the prenatal-to-postnatal transition.

The Most Dominant Modules for Gene Expression Changes Implicate Crucial Biological Processes Underlying Physiological Adaptions during the Prenatal-to-Postnatal Transition

Next, we respectively investigated the distribution of the *R* and MIC values across all 23 coexpression modules and found that M1 and M23 occupied the tailed regions (fig. 3*A* and supplementary fig. S3, Supplementary Material online), suggesting that M1 and M23 represent the most dominant modules containing the genes with the up- and down-regulated expression trajectories during development. Indeed, M1 and M23 generally displayed positive and negative correlations with the DDS across the developmental time points, especially at the perinatal stage (fig. 3*B* and supplementary fig. S3, Supplementary Material online). To confirm the dominance of M1 and M23 in gene expression changes around the perinatal stage compared with other modules, we performed the gene set enrichment analysis (GSEA) that can effectively identify gene sets differentiating two given groups by expression distribution (Subramanian et al. 2005). Among the top 200 GSEA up-regulated genes for differentiating the prenatal and postnatal stages (supplementary table S8,

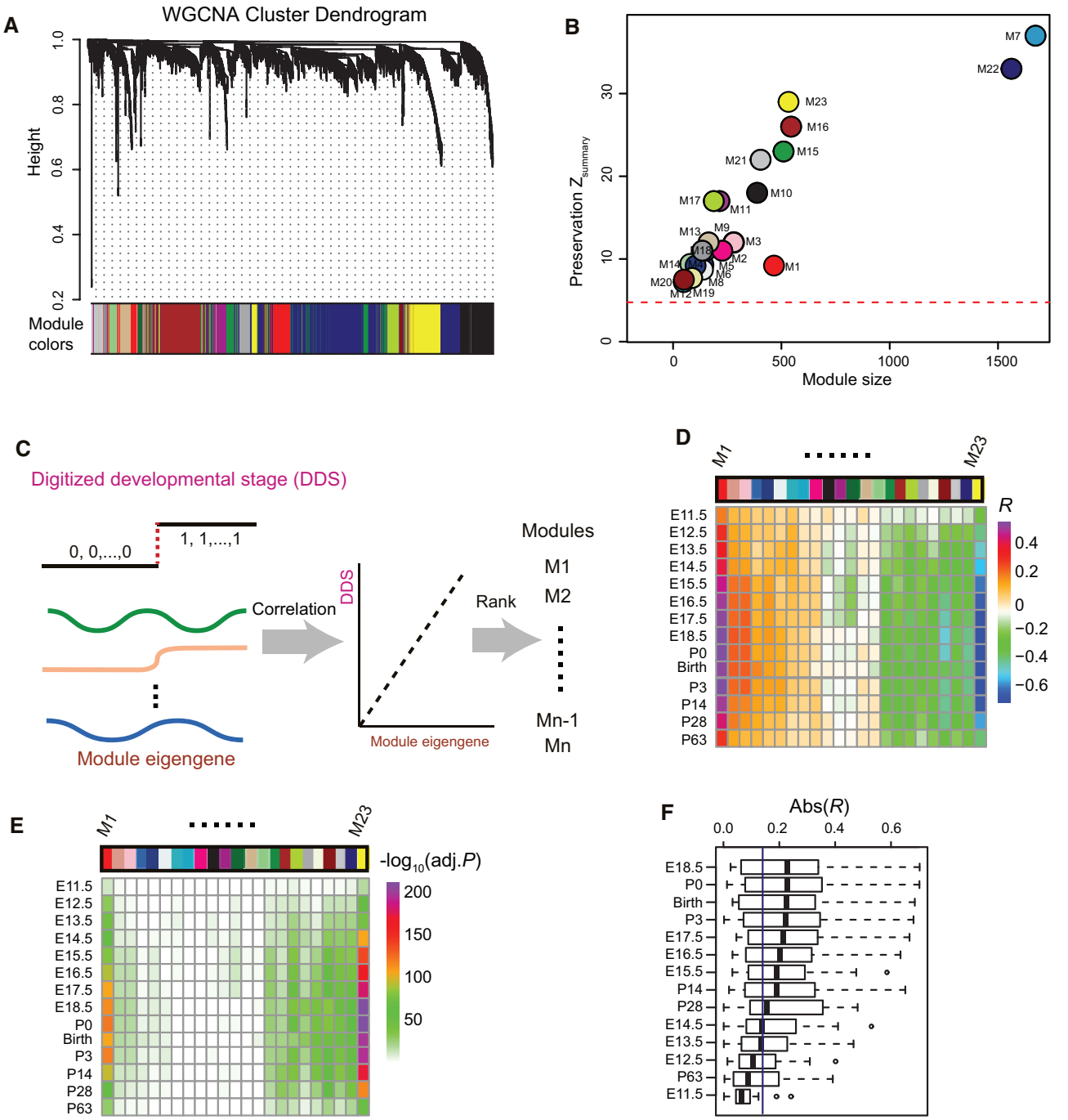

FIG. 2. Identification of key gene coexpression modules and developmental stages that relate to gene expression changes. (*A*) The clustering dendrogram of genes and the coexpression modules are assigned with colors. (*B*) The preservation test of 23 identified gene coexpression modules. The dashed line represents the cutoff of significant preservation ($Z_{summary}$=5). (*C*) The pipeline of identifying the gene coexpression modules correlated with the digitized developmental stages (DDSs). The modules are ranked by Person correlation coefficient (*R*) between ME and DDS for each developmental stage. Heatmap of *R* values (*D*) and the corresponding adjusted *P* values (*E*) for all 23 gene coexpression modules across 14 developmental stages. (*F*). The developmental stages are ranked by the median of the absolute values of *R* derived from 23 coexpression modules. The blue line represents the median of the absolute values of *R* on an average.

Supplementary Material online), M1 shared 17.4% (81/466) genes, which was significantly larger than random expectation ($P = 4.88 \times 10^{-51}$, hypergeometric test); M23 shared significantly more genes (27%, 144/533) with the top 200 GSEA down-regulated genes for differentiating the prenatal and postnatal stages than random expectations ($P = 2.89 \times 10^{-133}$; hypergeometric test). More importantly, the shared proportions of up-regulated and down-regulated genes for both M1 and M23 were significantly larger than those of other modules ($P < 0.001$; two-tailed χ^2 tests; supplementary fig. S4, Supplementary Material online). Thus, M1 and M23 are suggested to be the dominant coexpression

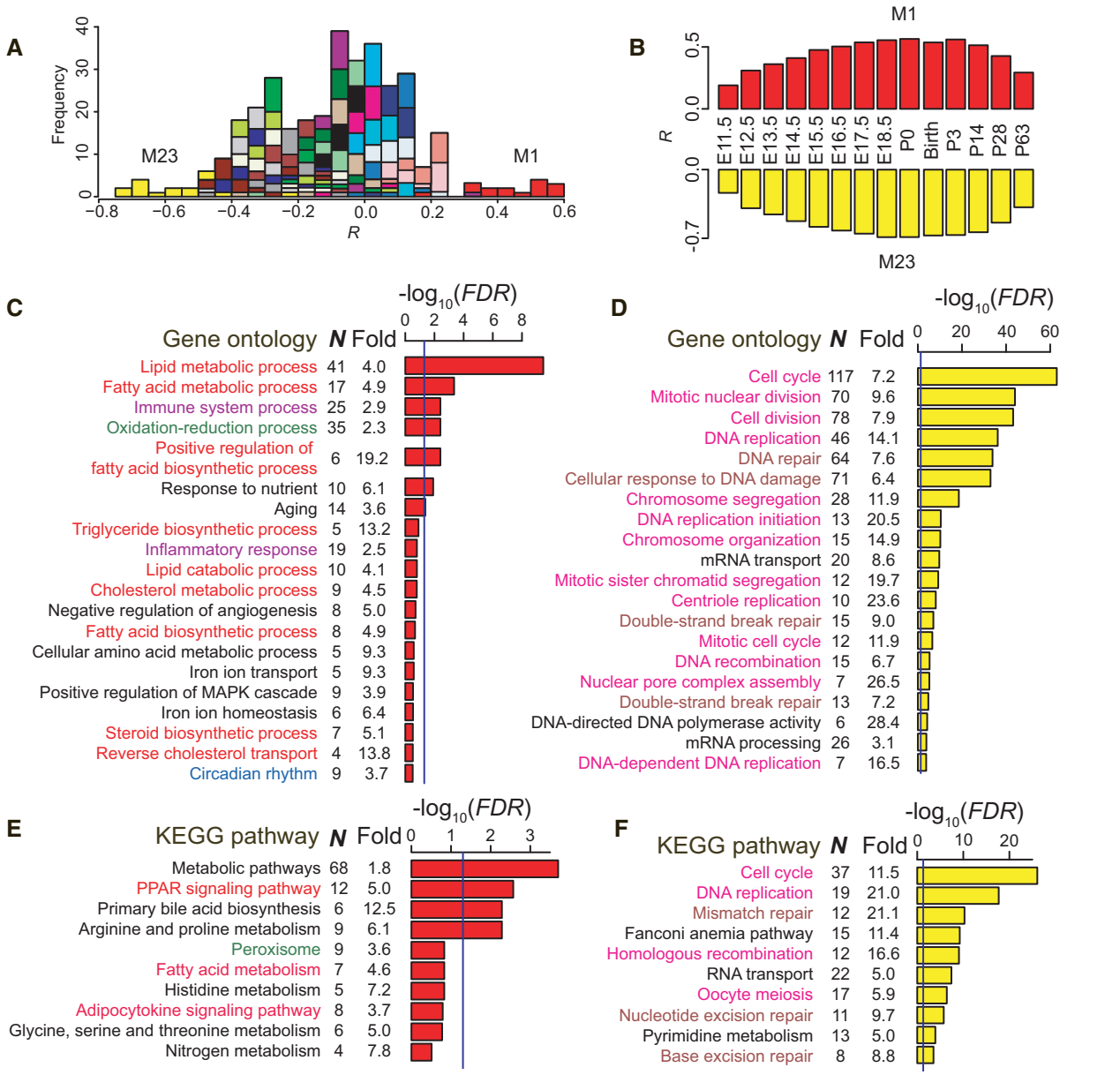

Fig. 3. Functional and pathway enrichment analyses for the most dominant up- and down-regulated modules. (*A*) Frequency distribution of *R* values correlated ME of each module with DDSs across the developmental stages. (*B*) The *R* values of M1 and M23 are shown for the developmental stages. The top 20 GO functional enrichment categories are shown for M1 (*C*) and M23 (*D*). The top 10 KEGG pathway enrichment terms are also shown for M1 (*E*) and M23 (*F*). The functionally relevant terms are highlighted with the same colors.

modules for the gene expression changes at the perinatal stage, representing two key modules with opposite gene expression trajectories across the developmental stages.

We further assessed the shared functions among the genes involved in the up-regulated module M1 by Gene Ontology (GO) enrichment analyses based on the DAVID platform (Huang Da et al. 2009). Of the top 20 significantly enriched GO biological process terms for the genes within the up-regulated module M1, there were 9 closely related to lipid metabolism and 2 related to immune response, as well as oxidation–reduction process (fig. 3C and supplementary table S9, Supplementary Material online). The genes involved in the down-regulated module M23 were enriched in 13 terms related to cell cycle and 4 terms related to DNA damage and repair (fig. 3D and supplementary table S10, Supplementary Material online). In addition, we also performed signaling pathway enrichment analyses for the genes within M1 and M23, respectively (supplementary tables S9 and S10, Supplementary Material online). Interestingly, the top 10 pathways for M1 included metabolic pathway, fatty acid metabolism, and adipocytokine signaling pathway (fig. 3E); the top 10 pathways for M23 included cell cycle, DNA replication, and homologous recombination (fig. 3F), which were highly consistent with the results of the GO enrichment analyses. Note that both the enhancement of lipid metabolism and the reduction of cell cycle may be relevant to the increase of oxygen concentration during the transition from fetuses to newborns (Girard et al. 1992; Puente et al. 2014). To test the

robustness of the modularity of M1 and M23 in gene number and species number, we performed the WGCNA analysis for 10,824 mouse-rat orthologous genes and 13,777 mouse-only genes, respectively (supplementary figs. S5 and S6 and table S11, Supplementary Material online). Among the gene coexpression modules, the positively correlated modules and the negatively correlated modules for both data sets shared significantly more genes with M1 and M23, respectively ($P < 10^{-43}$; hypergeometric test). More importantly, the GO and KEGG enrichment analyses for the genes within these modules showed highly consistent results with M1 and M23 (supplementary figs. S7 and S8 and tables S12–S15, Supplementary Material online).

Transcriptional Regulation for Physiological Adaptions during the Prenatal-to-Postnatal Transition

To investigate implications of transcription factors (TFs) in gene expression changes for physiological changes during the prenatal-to-postnatal transition, we conducted an enrichment analysis by screening the database of the TF-binding sites derived from the experimental chromatin immunoprecipitation data (Lachmann et al. 2010) for the genes within M1 and M23, respectively. For M1, there were 3 significantly enriched TFs (PPARA, IRF8, and NR1H3) that respectively regulate 24.5%, 15.9%, and 6.0% coexpressed genes (fig. 4A and supplementary table S16, Supplementary Material online). PPARs, including PPARA, PPARB, and PPARG, are responsive to fatty acid ligands and regulate the expression of genes involved in cellular lipid metabolism (Madrazo and Kelly 2008). Transgenic mice that overexpress PPARA show an increase in the expression of genes encoding key enzymes involved in fatty acid uptake and oxidation, concomitant with a decrease in the expression of glucose uptake and utilization genes (Finck et al. 2002), which appear to play important roles in coping with the fuel switching from glucose to lipid during the prenatal-to-postnatal transition. For M23, a total of 6 TFs (MYC, E2F1, FOXM1, MYBL2, TTF2, and E2F7) were significantly enriched for their binding sites among the coexpressed genes (fig. 4B and supplementary table S17, Supplementary Material online). Of these TFs, MYC regulated 53.3% of the coexpressed genes within M23, suggesting its crucial role on the gene regulatory network. MYC stimulates the cell cycle progression by inducing the expression of critical positive cell cycle regulators such as E2F TFs, Cdks, and cyclins, and the down-regulation or inactivation of MYC results in the impairment of cell cycle progression (Meyer and Penn 2008; Bretones et al. 2015). Beyond the hubs in the gene expression regulatory networks, these TFs generally exhibited evolutionarily conserved up- and down-regulated expression trajectories across five placental mammals and showed significant expression differences between prenatal and postnatal stages (fig. 4C), suggesting the important roles of the TFs on the physiological changes during the prenatal-to-postnatal transition.

Interestingly, these TFs, especially PPARA and MYC, were involved in the enriched signaling pathways (fig. 3E and F), namely PPAR signaling pathway and cell cycle pathway (fig. 4D and E). The two pathways can be organized into the broad categories of lipid metabolism, fatty acid transport, immune response, circadian rhythm, DNA replication, DNA repair, and mitotic cell cycle, which are all closely associated with the physiological changes during the prenatal-to-postnatal transition. In addition to the TFs, the expression changes of other genes in the pathways also exhibited significant correlations with the developmental trajectories and significant expression differences between the prenatal and postnatal stages (fig. 4F), further suggesting the functional importance of these pathways during the prenatal-to-postnatal transition.

The Toggle Switch Model for Gene Expression Changes during the Prenatal-to-Postnatal Transition

Individually investigating gene regulatory networks of the modules can reveal a detailed molecular basis underlying physiological adaptations during the prenatal-to-postnatal transition. However, the transition from prenatal to postnatal represents a systematically shifting process, accompanying the decline of some phenotypes and the enhancement of others. Given the opposite correlation of gene expression with the DDS between prenatal and postnatal stages, we hypothesized that the genetic toggle switch in the prenatal and the postnatal stages would maintain the flow of biological information during a state transition. A toggle switch refers to a mutually inhibitory pattern of the synthetic, bistable gene-regulatory, and protein–protein interaction networks (Gardner et al. 2000; Shiraishi et al. 2010). Taking a toggle switch gene pair (*a* and *b*) as an example, when the expression of the gene *a* increases (switch on) during the prenatal-to-postnatal transition, the expression of the gene *b* decrease (switch off) through their mutual negative regulation, and vice versa (fig. 5A). To test this hypothesis, we searched the toggle switch network data set (Shiraishi et al. 2010) using the genes involved in the modules. The ratio of the number of the observed toggle switch gene pairs to that of the total gene pairs was significantly larger between the down-regulated and up-regulated genes than both between down-regulated genes and between up-regulated genes, respectively ($P = 8.43 \times 10^{-53}$; $P = 2.97 \times 10^{-7}$; two-tailed χ^2 tests; fig. 5B). The opposite expression trends of two genes during development represent the highly consistent regulation pattern of mutual inhibition within a toggle switch gene pair (Shiraishi et al. 2010). We ranked a total of 785 toggle switch gene pairs by their correlation coefficient product, which reflects the amplitude of mutual inhibition between genes during the prenatal-to-postnatal transition (supplementary table S18, Supplementary Material online). Among the top 10 in the list, 5 toggle switch gene pairs were derived from the module pair M1–M23 that are precisely the most dominated modules of gene expression changes during the prenatal-to-postnatal transition (fig. 5C). Moreover, the correlation coefficient products of toggle switch gene pairs were significantly smaller for the module pair M1–M23 than for all other module pairs with the opposite expression trends ($P < 0.001$; Bootstrap test; fig. 5D), suggesting the larger

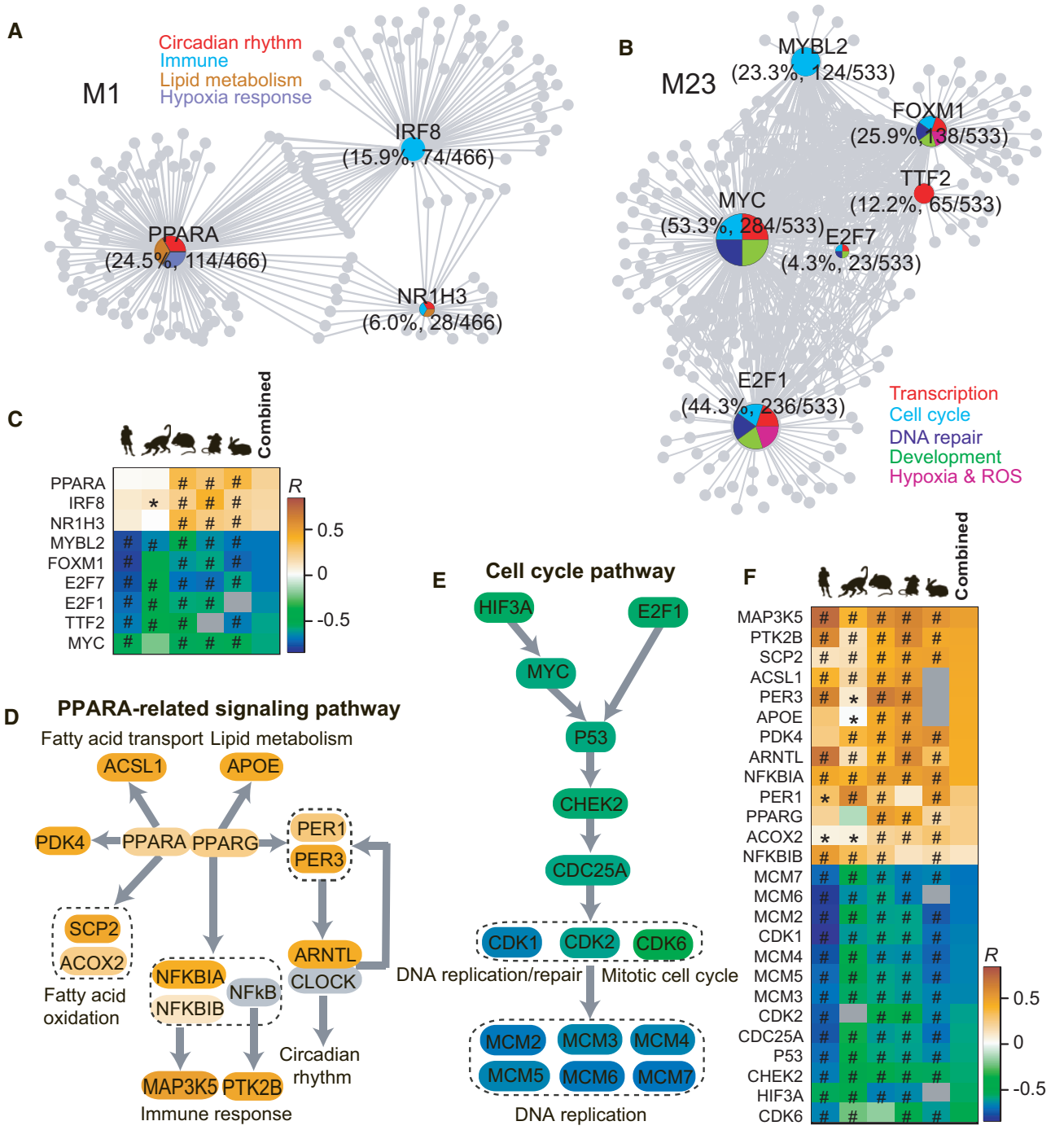

Fig. 4. Multiple TFs mediate gene coexpression networks and signaling pathways that relate to the biological functions in response to environmental changes during the prenatal-to-postnatal transition. Regulatory topology and functional annotations for the TFs in the TF-target network of M1 (*A*) and M23 (*B*). The size of the nodes is proportional to the degree of connectivity. (*C*) The heatmap of TFs based on *R* values between the ME and the DDS at the birth stage for each of five placental mammals and for their combined data set. These TFs are generally expressed differentially between the prenatal and postnatal stages. PPARA-related signaling pathway and cell cycle pathway are significantly enriched for M1 (*D*) and M23 (*E*), respectively. The node color denotes the scale of *R* values. (*F*) The *R* heatmap of the genes involved in the two signaling pathways above. They are also generally expressed differentially between the prenatal and postnatal stages. The *P* values are from two-tailed Student's *t*-tests. $^{*}P < 0.05$, $^{\#}P < 0.01$.

amplitude of mutual inhibition for the module pair M1–M23 than for other module pairs. To confirm the toggle switch model, we used the pairs of transcription factors (TF–TF pairs) with the mutual binding motif as an independent test database because they competitively bind to a common specific DNA region (supplementary table S19, Supplementary Material online). Similarly, the ratio of the number of the observed toggle switch TF–TF pairs to that

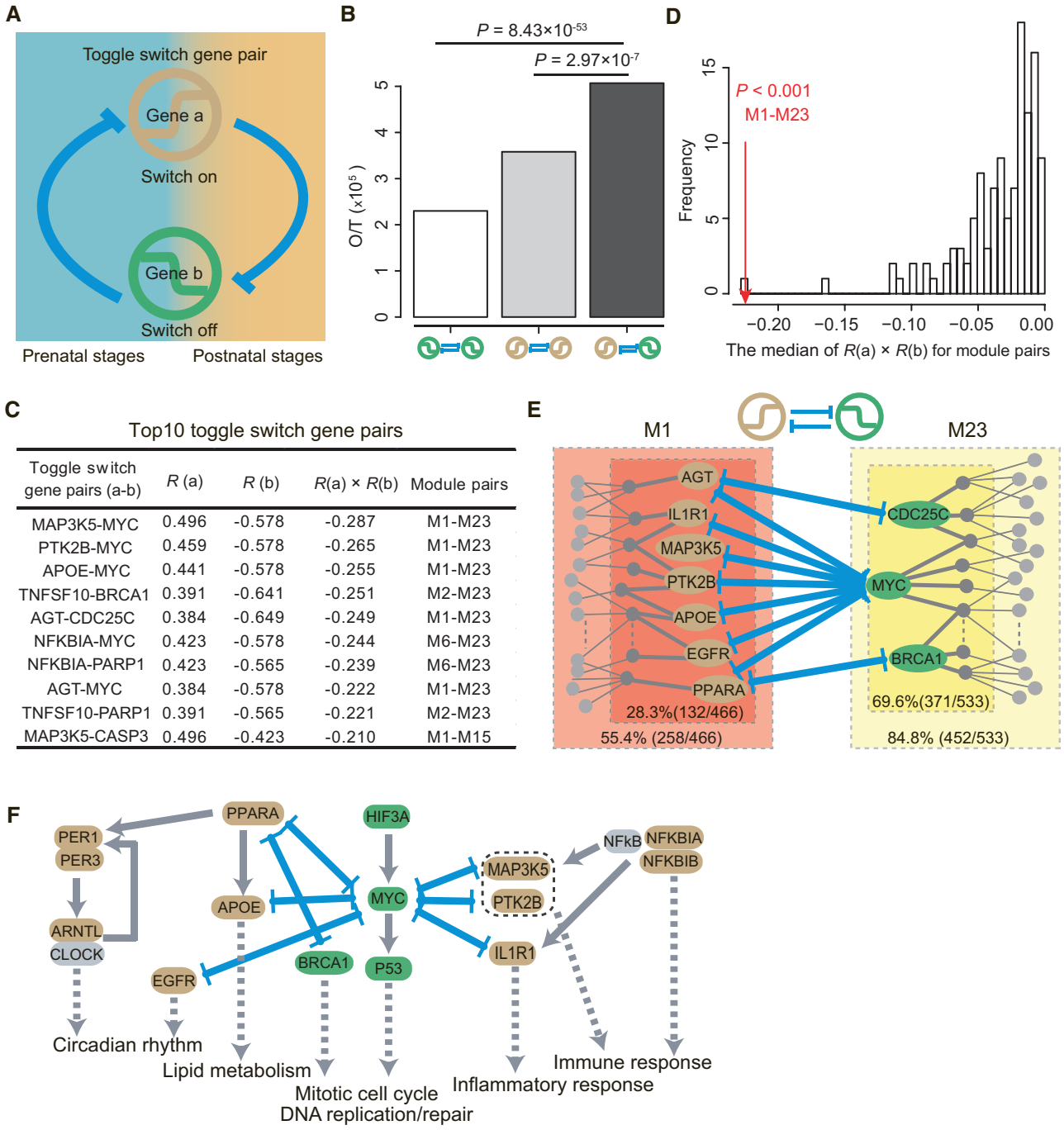

Toggle switch gene pairs (a-b)	R (a)	R (b)	R(a) × R(b)	Module pairs
MAP3K5-MYC	0.496	-0.578	-0.287	M1-M23
PTK2B-MYC	0.459	-0.578	-0.265	M1-M23
APOE-MYC	0.441	-0.578	-0.255	M1-M23
TNFSF10-BRCA1	0.391	-0.641	-0.251	M2-M23
AGT-CDC25C	0.384	-0.649	-0.249	M1-M23
NFKBIA-MYC	0.423	-0.578	-0.244	M6-M23
NFKBIA-PARP1	0.423	-0.565	-0.239	M6-M23
AGT-MYC	0.384	-0.578	-0.222	M1-M23
TNFSF10-PARP1	0.391	-0.565	-0.221	M2-M23
MAP3K5-CASP3	0.496	-0.423	-0.210	M1-M15

FIG. 5. The toggle switch model for the gene expression changes during the prenatal-to-postnatal transition. (*A*) The model of the toggle switch gene pair (e.g., gene *a* and gene *b*) for the prenatal-to-postnatal gene expression changes. (*B*) Three types of toggle switch gene pairs (down–down, up–up, and up–down) based on the expression trends along the developmental time points are compared by the ratio of the number of the observed gene pairs to the total number of gene pairs (O/T). The *P* values are from two-tailed χ^2 tests. (*C*) Top 10 up–down toggle switch gene pairs that are ranked by the product of their *R* values. (*D*) The median frequency distribution of the product of *R* values across all module pairs with anticorrelation. The *P* value for the module pair M1–M23 is from the Bootstrap test. (*E*) The genes involved in the toggle switch gene pairs are coexpressed with the majority of genes in M1 and M23. The inner and outer boxes denote the first and second neighbors in the coexpression networks, respectively. The blue lines represent the mutual inhibition in the toggle switch gene pairs. The gray lines denote the coexpression relationship. (*F*) The gene regulatory networks are mediated by the toggle switch gene pairs during the prenatal-to-postnatal transition.

of the total TF–TF pairs was significantly larger between the down-regulated and up-regulated TF–TF pairs than both between down-regulated TF–TF pairs and between up-regulated TF–TF pairs, respectively ($P = 1.19 \times 10^{-91}$; $P = 4.18 \times 10^{-6}$; two-tailed χ^2 tests; supplementary fig. S9A, Supplementary Material online). The correlation coefficient products of toggle switch TF–TF pairs were significantly smaller for the module pair M1–M23 than for all other

module pairs with the opposite expression trends ($P = 0.0017$; Bootstrap test; supplementary fig. S9B, Supplementary Material online).

In particular, 7 genes involved in the 9 toggle switch gene pairs in M1 had 132 first neighbors (28.3%) and 258 second neighbors (55.4%) in the gene coexpression network; 3 genes in the 9 toggle switch gene pairs in M23 owned 371 first neighbors (69.6%) and 452 second neighbors (84.8%) in the gene coexpression network (fig. 5E). More interestingly, the key TFs in the gene regulatory networks enriched in both M1 and M23 (fig. 4D and E) were also linked by the toggle switch gene pairs, suggesting the potentially crucial roles of the toggle switch gene pairs for the coordination in responses to the switching of multiple environmental factors during the prenatal-to-postnatal transition, such as oxygen tension, fat-rich diet, light–dark cycle, and foreign microbes (fig. 5F). Specifically, MYC is a key factor mediating 6 toggle switch gene pairs to connect the gene regulatory networks, and oxygen tension has important effects on the expression of the TFs PPARA and HIF3A, as well as on the ROS production, which subsequently regulates the expression of MYC (Forristal et al. 2010; Wong et al. 2013; Brew and Sullivan 2017). Mammals are born with an immature circadian rhythm and the light–dark cycle plays a critical role in the development of circadian rhythm by regulating the expression of the clock genes, including PER1, PER3, and ARNTL (Ciarleglio et al. 2011; Brooks et al. 2014). In addition to oxygen tension and light–dark cycle, exposure to foreign microbes can activate NF-κB proteins, subsequently inducing the expression of a broad spectrum of antimicrobial pro-inflammatory cellular response genes (Finlay and McFadden 2006; Hayden and Ghosh 2008; Rahman and McFadden 2011). Thus, beyond the intrinsic programs, the environmental factors switching from prenatal to postnatal stages likely induce the expression of the genes involved in the toggle switch gene pairs to mediate the gene expression regulatory networks underlying the physiological adaptations during the prenatal-to-postnatal transition, but the extent to which is needed to assess in future studies. In addition, it is of note that we only examined the toggle switch gene pairs between the two most positively and negatively correlated modules, and such gene pairs likely exist between other modules with the opposite gene expression pattern. Our analyses showed a general pattern of organ RNA profiles across developmental stages, which thus was not necessarily relevant to the particular developmental stage and cell type. As data accumulate, our hypothesis of the toggle switch of gene expression for the prenatal-to-postnatal transition would be further tested and expanded to the single-cell level.

Conclusion

The hourglass model has long been proposed to explain why embryogenesis diverges more extensively early and late than in the middle across nearly all animals and provides an attractive framework for understanding the molecular basis of this evolutionarily conserved developmental phenomenon from a molecular perspective (Duboule 1994; Domazet-Loso and Tautz 2010; Kalinka et al. 2010; Irie and Kuratani 2011; Hu et al. 2017). However, the perinatal stage, as one of the most dynamic and challenging developmental processes, is ignored for a long time, during which newborns have to independently face the dramatic environmental shifts compared with the fetuses completely depending on another for life-sustaining materials. In this study, we found the gene expression changes at the transcriptomic scale in multiple organs across five placental mammals during the perinatal stage. The enrichment analyses of gene function and gene expression regulatory networks for the genes involved in the up- and down-regulated coexpression modules reveal their close correlations with the physiological adaptations to the environmental changes during the prenatal-to-postnatal transition, such as oxygen concentration, nutrients, light–dark cycle, and foreign microbes. Further, we proposed the toggle switch model to explain the coordination between the genes involved in the coexpression modules with the opposite expression trajectories between the prenatal and postnatal stages, suggesting that the molecular contributions to the physiological adaptions during the perinatal stage have been deeply embedded in the developmental program during evolution. Nevertheless, it is of note that the toggle switch model is largely supported by bioinformatics and statistical analyses, but the functional data are needed to help strengthen the reliability and robustness of the model in future.

Materials and Methods

Sample Collection

We retrieved the gene expression data (RPKM; reads per kilobase of transcript, per million mapped reads) of seven organs (brain, cerebellum, heart, liver, kidney, ovary, and testes) across five placental mammals (human *Homo sapiens*, rhesus macaque *Macaca mulatta*, mouse *Mus musculus*, rat *Rattus norvegicus*, and rabbit *Oryctolagus cuniculus*), which spanned the prenatal, birth, and postnatal stages (Cardoso-Moreira et al. 2019). Due to lacking the postnatal ovary data for rhesus macaque and human, we obtained a total of 1,425 samples and 33 data sets for the placental mammals (supplementary table S1, Supplementary Material online). If the RPKM value of a gene is <0.5 in more than half of the samples for each data set, it will be discarded. Further, the retained data were normalized by the basic population and global normalization (Yang et al. 2002). Finally, a total of 12,425 genes were obtained across these data sets on an average. The gene expression levels were logarithmically transformed, $\log_2(\text{RPKM} + 1)$, for further analyses.

Principal Component Analysis and Curve Fitting

The function prcomp from *R* (ver.3.61) was used to perform the PCA for both all expressed genes and the variably expressed genes (CV$>$1) of each of 33 data sets across seven organs of five placental mammals (Venables and Ripley 2002). For each data set, the proportion of variance of PCA and the first five principal components were estimated (supplementary table S2, Supplementary Material online). The first two principal components (PC1 and PC2) were separately

averaged to represent the overall contribution of expression variance. The *R* function "lm($y \sim$ poly(x, poly_n))" was used to perform the polynomial curve fitting between PC1 and PC2. We estimated three fitting statistics: R^2, adjusted R^2, and the corresponding *P* value for each sample by respectively setting the parameter poly_n = 2, 3, and 4. Because the *P* values were generally minimal when poly_n = 3, this parameter was defined as the best polynomial fitting degree.

Weighted Gene Coexpression Network Analysis

We used the *R* package WGCNA (Langfelder and Horvath 2008) to construct coexpression networks for an integrated expression matrix of a total of 8,238 one-to-one orthologous protein-coding genes in at least four of five placental mammals from 1,425 samples described above. We logarithmically transformed the gene expression levels and found no mitochondrial genes in our data set, which largely reduced the impact of outliers on the analyses due to their excessive expression. First, the function "hclust()" was used to perform a hierarchical cluster analysis to detect the consistency of samples, and no outlier was found in the samples (supplementary fig. S2*A*, Supplementary Material online). Second, the scale-free topology model fit and the mean connectivity were estimated for each of soft-thresholding powers from 1 to 30. When the threshold power was equal to 18, both the topology model fit and the mean connectivity tended to be stable (supplementary fig. S2*B* and *C*, Supplementary Material online). Third, the function "blockwiseModules()" was used for network construction and module detection (power = 18, networkType="signed," minModuleSize = 30, mergeCutHeight = 0.25) and 23 gene coexpression modules were identified (fig. 2*A*). The gene coexpression modules in WGCNA were defined as branches of a hierarchical cluster tree using the top-down dynamic tree cut method and the coexpression modules comprised positively correlated genes with high topological overlap (Zhang and Horvath 2005; Langfelder et al. 2008). To assess the preservation of modules, we used the function "modulePreservation" built in the WGCNA (Langfelder et al. 2011) to analyze a control data set that contains the expression data of the same 8,238 genes from four organs (forebrain, heart, liver, and kidney) in the mouse ENCODE project and spanning E11.5 to 8 weeks (He et al. 2020). The quantitative measure of module preservation enables to test whether a module is preserved compared with the control data set based on the permutation test. Besides the one-to-one orthologous protein-coding genes across five mammals, we also performed the WGCNA analyses for 10,824 moue-rat orthologous genes and for 13,777 mouse-only genes.

Identifying Coexpression Modules with Gene Expression Switching for Each Developmental Time Point

For each of 15 mouse-matched developmental stages (E10.5, E11.5, E12.5, E13.5, E14.5, E15.5, E16.5, E17.5, E18.5, P0, birth, P3, P14, P28, and P63) (Cardoso-Moreira et al. 2019), we digitized the developmental stages (DDS) before and after the given stage by the binary digits "0" and "1," respectively. Notably, because E10.5 was the first stage in our data set and no stage was before it, then the DDS of E10.5 was assigned to all "1" and thus its correlation with gene coexpression modules cannot be estimated. Finally, the DDS matrixes containing 0 and 1 were obtained to index the switching specificity of developmental phenotypes. For each coexpression module, the expression patterns were summarized by the ME, defined as the right singular vector of the standardized expression patterns. We used the function *cor* in WGCNA to estimate the Pearson correlation coefficient (*R*) as the correlation strength between ME and DDS for each developmental time point. $R > 0$ means that the general expression of the module is positively correlated with the DDS; otherwise, it is negatively correlated. Meanwhile, the corresponding *P* values are calculated by the function *corPvalueStudent* in WGCNA. Except for the Pearson correlation coefficient, we also calculated the MIC to estimate the nonlinear correlation strength between ME and DDS using the function MINE in the R package minerva (Reshef et al. 2011) with alpha = 1. MIC can effectively detect the nonlinear correlation between variables. MIC approaching 1 means a stronger nonlinear correlation between ME and DDS.

Gene Set Enrichment Analysis for the Prenatal and Postnatal Stages

We used GSEA (version 4.0.3) with the "Signal2Noise" ranking metric and a threshold nominal $P < 0.05$ (Subramanian et al. 2005) to identify gene sets that show different expression levels between the prenatal and postnatal stages. After being ranked according to the enrichment score, the genes that significantly distinguish the prenatal and postnatal stages were tended to locate at the top (up-regulated) and bottom (down-regulated) of the list. The top up-regulated and down-regulated 200 genes were selected to overlap with the genes from each of 23 coexpression modules, respectively. We performed the hypergeometric tests to estimate the statistical significance for the overlapping.

Enrichment Analyses for Gene Functions and Signaling Pathways

DAVID version 6.8 (Huang Da et al. 2009) was used to perform GO and Kyoto Encyclopedia of Genes and Genomes (KEGG) signaling pathway enrichment analyses. The selected genes were uploaded as input and all corresponding protein-coding genes were used as the background.

Transcription Factor Binding Site Enrichment Analysis and Gene Regulatory Network Construction

All coexpressed genes in M1 and M23 were used for TF-binding motif enrichment analyses, respectively (Kuleshov et al. 2016). The relationships between TFs and targets were retrieved from the gene set library based on the database of genome-wide chromatin immunoprecipitation sequencing (ChIP-seq), where the peaks at the promoters of target genes were detected with a 400-bp sliding window (Lachmann et al. 2010). Only TFs with adjusted $P < 0.05$ are considered enriched and their functions were annotated with GO terms.

Finally, the gene regulatory networks were drawn with Cytoscape (v3.7.1) (Shannon et al. 2003).

Identification of Toggle Switch Gene Pairs among Coexpressed Genes

We mapped the coexpressed genes into an integrated toggle switch network (Shiraishi et al. 2010) that contains 6,585 toggle switch gene pairs. According to the sign of Pearson's correlation coefficient (R), we classified the identified toggle switch gene pairs into three types: up–down, down–down, and up–up. To identify the toggle switch gene pairs that contribute most to gene expression changes, we computed an amplitude index by multiplying the Pearson's correlation coefficients of two genes within a pair at the Birth stage. For the up–down toggle switch gene pairs, the amplitude indexes were always negative; the smaller, the greater contribution to the gene expression changes. In addition, we compiled a data set containing TFs with the mutual binding motif based on two TF databases Homer (homer.ucsd.edu/homer) and Jaspar (jaspar.genereg.net). After mapping all coexpressed genes into the data set, we identified a total of 1,645 TF–TF pairs with the mutual binding motif (supplementary table S19, Supplementary Material online). Then, the similar analyses above were performed to test the toggle switch model according to different types of gene expression.

Supplementary Material

Supplementary data are available at *Molecular Biology and Evolution* online.

Acknowledgments

We thank two anonymous reviewers and Yong Wang for his very helpful suggestions for collecting samples. The project was supported by grants from the Strategic Priority Research Program of the Chinese Academy of Sciences (XDPB17), National Key Research and Development Program of China (2021YFC2301300 and 2020YFC0847000), National Natural Science Foundation of China (31930011, 31922010, 32192422, and 31871270), Yunnan Provincial Science and Technology Department (2019FI008), and the Key Research Program of the Chinese Academy of Sciences (KJZD-SW-L11).

Author Contributions

P.S., Z.L., and J.-J.H. designed the research. W.-L.H. performed the sample collection and data preprocessing. J.-J.H. analyzed the data. Z.L., J.-J.H., and P.S. wrote and revised the paper.

Data Availability

The data underlying this article are available in Kaessmann Lab, at http://evodevoapp.kaessmannlab.org. Computer code, parameters, and intermediate results are available upon request.

References

Asikainen TM, Raivio KO, Saksela M, Kinnula VL. 1998. Expression and developmental profile of antioxidant enzymes in human lung and liver. *Am J Respir Cell Mol Biol*. 19(6):942–949.

Askin DF. 2002. Complications in the transition from fetal to neonatal life. *J Obstet Gynecol Neonatal Nurs*. 31(3):318–327.

Battaglia FC, Meschia G. 1978. Principal substrates of fetal metabolism. *Physiol Rev*. 58(2):499–527.

Bretones G, Delgado MD, Leon J. 2015. Myc and cell cycle control. *Biochim Biophys Acta*. 1849(5):506–516.

Brew O, Sullivan MHF. 2017. Oxygen and tissue culture affect placental gene expression. *Placenta* 55:13–20.

Brooks E, Patel D, Canal MM. 2014. Programming of mice circadian photic responses by postnatal light environment. *PLoS One* 9(5):e97160.

Cardoso-Moreira M, Halbert J, Valloton D, Velten B, Chen C, Shao Y, Liechti A, Ascencao K, Rummel C, Ovchinnikova S, et al. 2019. Gene expression across mammalian organ development. *Nature* 571(7766):505–509.

Carrasco M, Martell M, Estol PC. 1997. Oronasopharyngeal suction at birth: effects on arterial oxygen saturation. *J Pediatr*. 130(5):832–834.

Catt JW, Henman M. 2000. Toxic effects of oxygen on human embryo development. *Hum Reprod*. 15(Suppl 2):199–206.

Chapple RH, Tizioto PC, Wells KD, Givan SA, Kim J, McKay SD, Schnabel RD, Taylor JF. 2013. Characterization of the rat developmental liver transcriptome. *Physiol Genomics*. 45(8):301–311.

Ciarleglio CM, Axley JC, Strauss BR, Gamble KL, McMahon DG. 2011. Perinatal photoperiod imprints the circadian clock. *Nat Neurosci*. 14(1):25–27.

Dimich I, Singh PP, Adell A, Hendler M, Sonnenklar N, Jhaveri M. 1991. Evaluation of oxygen-saturation monitoring by pulse oximetry in neonates in the delivery system. *Can J Anaesth*. 38(8):985–988.

Domazet-Loso T, Tautz D. 2010. A phylogenetically based transcriptome age index mirrors ontogenetic divergence patterns. *Nature* 468(7325):815–818.

Duboule D. 1994. Temporal colinearity and the phylotypic progression: a basis for the stability of a vertebrate Bauplan and the evolution of morphologies through heterochrony. *Dev Suppl*. 1994(Suppl):135–142.

Emmanouilides G, Allen H, Riemenschneider T, Gutgesell H. 1995. Moss and Adams' heart disease in infants, children, and adolescents: including the fetus and young adult. 5 ed. Baltimore (MD): Williams & Wilkins.

Eppig JJ, Wigglesworth K. 1995. Factors affecting the developmental competence of mouse oocytes grown in vitro: oxygen concentration. *Mol Reprod Dev*. 42(4):447–456.

Finck BN, Lehman JJ, Leone TC, Welch MJ, Bennett MJ, Kovacs A, Han X, Gross RW, Kozak R, Lopaschuk GD, et al. 2002. The cardiac phenotype induced by PPARalpha overexpression mimics that caused by diabetes mellitus. *J Clin Invest*. 109(1):121–130.

Finlay BB, McFadden G. 2006. Anti-immunology: evasion of the host immune system by bacterial and viral pathogens. *Cell* 124(4):767–782.

Forristal CE, Wright KL, Hanley NA, Oreffo ROC, Houghton FD. 2010. Hypoxia inducible factors regulate pluripotency and proliferation in human embryonic stem cells cultured at reduced oxygen tensions. *Reproduction* 139(1):85–97.

Gardner TS, Cantor CR, Collins JJ. 2000. Construction of a genetic toggle switch in *Escherichia coli*. *Nature* 403(6767):339–342.

Girard J, Ferre P, Kervran A, Pegorier J, Assan R. 1977. Influence of insulin/glucagon ratio in the changes of hepatic metabolism during development of the rat. In: Foa PP, Bajaj JS, Foa NL, editors. Glucagon: its role in physiology and clinical medicine. Amsterdam: Excerpta Med. p. 563–581.

Girard J, Ferre P, Pegorier J, Duee P. 1992. Adaptations of glucose and fatty acid metabolism during perinatal period and suckling-weaning transition. *Physiol Rev*. 72(2):507–541.

Girard JR, Cuendet GS, Marliss EB, Kervran A, Rieutort M, Assan R. 1973. Fuels, hormones, and liver metabolism at term and during the early postnatal period in the rat. *J Clin Invest*. 52(12):3190–3200.

Han X, Wu X, Chung WY, Li T, Nekrutenko A, Altman NS, Chen G, Ma H. 2009. Transcriptome of embryonic and neonatal mouse cortex by

high-throughput RNA sequencing. *Proc Natl Acad Sci U S A*. 106(31):12741–12746.
Harris AP, Sendak MJ, Donham RT. 1986. Changes in arterial oxygen-saturation immediately after birth in the human neonate. *J Pediatr*. 109(1):117–119.
Hayden MS, Ghosh S. 2008. Shared principles in NF-kappa B signaling. *Cell* 132(3):344–362.
He Y, Hariharan M, Gorkin DU, Dickel DE, Luo C, Castanon RG, Nery JR, Lee AY, Zhao Y, Huang H, et al. 2020. Spatiotemporal DNA methylome dynamics of the developing mouse fetus. *Nature* 583(7818):752–759.
Henning SJ. 1981. Postnatal development: coordination of feeding, digestion, and metabolism. *Am J Physiol*. 241(3):G199–G214.
Honma S. 2020. Development of the mammalian circadian clock. *Eur J Neurosci*. 51(1):182–193.
Hu HY, Uesaka M, Guo S, Shimai K, Lu TM, Li F, Fujimoto S, Ishikawa M, Liu SP, Sasagawa Y, et al. 2017. Constrained vertebrate evolution by pleiotropic genes. *Nat Ecol Evol*. 1(11):1722–1730.
Huang Da W, Sherman BT, Lempicki RA. 2009. Systematic and integrative analysis of large gene lists using DAVID bioinformatics resources. *Nat Protoc*. 4(1):44–57.
Hurley E, Zabala V, Boylan JM, Gruppuso PA, Sanders JA. 2018. Hepatic gene expression during the perinatal transition in the rat. *Gene Expr*. 19(1):1–13.
Irie N, Kuratani S. 2011. Comparative transcriptome analysis reveals vertebrate phylotypic period during organogenesis. *Nat Commun*. 2:248.
Kalinka AT, Varga KM, Gerrard DT, Preibisch S, Corcoran DL, Jarrells J, Ohler U, Bergman CM, Tomancak P. 2010. Gene expression divergence recapitulates the developmental hourglass model. *Nature* 468(7325):811–814.
Kuleshov MV, Jones MR, Rouillard AD, Fernandez NF, Duan Q, Wang Z, Koplev S, Jenkins SL, Jagodnik KM, Lachmann A, et al. 2016. Enrichr: a comprehensive gene set enrichment analysis web server 2016 update. *Nucleic Acids Res*. 44(W1):W90–97.
Lachmann A, Xu H, Krishnan J, Berger SI, Mazloom AR, Ma'ayan A. 2010. ChEA: transcription factor regulation inferred from integrating genome-wide ChIP-X experiments. *Bioinformatics* 26(19):2438–2444.
Langfelder P, Horvath S. 2008. WGCNA: an R package for weighted correlation network analysis. *BMC Bioinformatics* 9(1):9.
Langfelder P, Luo R, Oldham MC, Horvath S. 2011. Is my network module preserved and reproducible? *PLoS Comput Biol*. 7(1):e1001057.
Langfelder P, Zhang B, Horvath S. 2008. Defining clusters from a hierarchical cluster tree: the dynamic tree cut package for R. *Bioinformatics* 24(5):719–720.
Madrazo JA, Kelly DP. 2008. The PPAR trio: regulators of myocardial energy metabolism in health and disease. *J Mol Cell Cardiol*. 44(6):968–975.
Meyer N, Penn LZ. 2008. Reflecting on 25 years with MYC. *Nat Rev Cancer*. 8(12):976–990.
Mota-Rojas D, Orozco-Gregorio H, Villanueva-Garcia D, Bonilla-Jaime H, Suarez-Bonilla X, Hernandez-Gonzalez R, Roldan-Santiago P, Trujillo-Ortega ME. 2011. Foetal and neonatal energy metabolism in pigs and humans: a review. *Vet Med*. 56(5):215–225.
Oski FA, Delivoria-Papadopoulos M. 1971. The shift to the left. *Pediatrics* 48(6):853–856.
Pabon JE Jr, Findley WE, Gibbons WE. 1989. The toxic effect of short exposures to the atmospheric oxygen concentration on early mouse embryonic development. *Fertil Steril*. 51(5):896–900.
Platt MW, Deshpande S. 2005. Metabolic adaptation at birth. *Semin Fetal Neonatal Med*. 10(4):341–350.
Porter KB. 1987. Evaluation of arterial oxygen saturation of the newborn in the labor and delivery suite. *J Perinatol*. 7(4):337–339.
Puente BN, Kimura W, Muralidhar SA, Moon J, Amatruda JF, Phelps KL, Grinsfelder D, Rothermel BA, Chen R, Garcia JA, et al. 2014. The oxygen-rich postnatal environment induces cardiomyocyte cell-cycle arrest through DNA damage response. *Cell* 157(5):1243–1243.
Rahman MM, McFadden G. 2011. Modulation of NF-kappa B signalling by microbial pathogens. *Nat Rev Microbiol*. 9(4):291–306.
Reshef DN, Reshef YA, Finucane HK, Grossman SR, McVean G, Turnbaugh PJ, Lander ES, Mitzenmacher M, Sabeti PC. 2011. Detecting novel associations in large data sets. *Science* 334(6062):1518–1524.
Shannon P, Markiel A, Ozier O, Baliga NS, Wang JT, Ramage D, Amin N, Schwikowski B, Ideker T. 2003. Cytoscape: a software environment for integrated models of biomolecular interaction networks. *Genome Res*. 13(11):2498–2504.
Shiraishi T, Matsuyama S, Kitano H. 2010. Large-scale analysis of network bistability for human cancers. *PLoS Comput Biol*. 6(7):e1000851.
Subramanian A, Tamayo P, Mootha VK, Mukherjee S, Ebert BL, Gillette MA, Paulovich A, Pomeroy SL, Golub TR, Lander ES, et al. 2005. Gene set enrichment analysis: a knowledge-based approach for interpreting genome-wide expression profiles. *Proc Natl Acad Sci U S A*. 102(43):15545–15550.
Torres-Cuevas I, Parra-Llorca A, Sanchez-Illana A, Nunez-Ramiro A, Kuligowski J, Chafer-Pericas C, Cernada M, Escobar J, Vento M. 2017. Oxygen and oxidative stress in the perinatal period. *Redox Biol*. 12:674–681.
Venables WN, Ripley BD. 2002. Modern applied statistics with S. New York: Springer-Verlag.
Villamor E, Moreno L, Mohammed R, Perez-Vizcaino F, Cogolludo A. 2019. Reactive oxygen species as mediators of oxygen signaling during fetal-to-neonatal circulatory transition. *Free Radic Biol Med*. 142:82–96.
Wong WJ, Qiu B, Nakazawa MS, Qing GL, Simon MC. 2013. MYC degradation under low O2 tension promotes survival by evading hypoxia-induced cell death. *Mol Cell Biol*. 33(17):3494–3504.
Yang YH, Dudoit S, Luu P, Lin DM, Peng V, Ngai J, Speed TP. 2002. Normalization for cDNA microarray data: a robust composite method addressing single and multiple slide systematic variation. *Nucleic Acids Res*. 30:e15.
Yu JC, Khodadadi H, Malik A, Davidson B, Salles E, Bhatia J, Hale VL, Baban B. 2018. Innate immunity of neonates and infants. *Front Immunol*. 9:1759.
Zhang B, Horvath S. 2005. A general framework for weighted gene co-expression network analysis. *Stat Appl Genet Mol Biol*. 4(1):17.